Chapter 4

Monte-Carlo simulation of physical sources

In this chapter I describe the Monte-Carlo simulation used to generate the processes which are known to contribute to the intermediate mass region of the dimuon mass spectrum. These are the DY process and the semi-leptonic decays of charmed hadron pairs. The high mass resonance simulation is also described since both the J/ψ and the ψ' are needed in the following analysis (see chapter 6) and since the reconstructed J/ψ partially contributes to the IMR dimuon yield. The generated processes are reconstructed using the same dedicated program which has been used to reconstruct the data. The Monte-Carlo mass differential distributions are fitted with ad-hoc functions. The same functions will be used in chapter 6 in the fit of the experimental mass spectrum. The latter is in fact a superposition of the above listed different processes, the relative contribution of which can be only determined by mean of a fit of the experimental mass spectrum itself. The contribution of the combinatorial background from pion and kaon decays, which is one of the most important source of (fake) dimuons in the IMR, will be separately discussed in chapter 5.

4.1 Introduction

The dimuon invariant mass spectrum is a convolution of contributions from different physical sources. The differential distributions of the contributing processes are obtained with the use of Monte-Carlo simulations which take into account the theoretical knowledge about the processes them-self plus the deforming action of the experimental apparatus on the shapes of the generated differential distributions. This is accomplished generating the theoretical shapes with a dedicated program[1], whilst for the reconstruction the same program used to reconstruct experimental data is used[2]. Kinematic cuts, which were already discussed in chapter 3, are also applied on the reconstructed spectra, that is

$$0 < y^* < 1 \tag{4.1}$$

$$-0.5 < cos\theta_{CS} < 0.5 \tag{4.2}$$

for the PbPb and SU set-ups and

$$-0.52 < y^* < 0.48 \tag{4.3}$$

$$-0.5 < cos\theta_{CS} < 0.5 \tag{4.4}$$

for the 4 pA ones. A respective 1% and 18% PXDTARG selection (see chapter 3) has also been applied on the pA and PbPb data.

Once the reconstructed differential distributions have been obtained, they are fitted with ad-hoc functions. The same functions are then used in the fit of the experimental mass spectrum. When fitting the experimental mass spectrum, the normalisation factors are left as free parameters. If needed, some other parameters can be also left free, as explained in the chapter 6.

4.2 The Monte-Carlo DY generation

The DY differential distributions have been generated with the following parametrisations :

- *Mass and rapidity differential distribution*

  The leading order pQCD DY cross section has been used (see chapter 1), i.e.

$$M^3 \frac{d^2\sigma}{dMdy^*} = \frac{8\pi\alpha^2}{9}\tau \sum_i e_i^2[f_1^i(\sqrt{\tau}e^{y^*})\overline{f}_2^i(\sqrt{\tau}e^{-y^*}) + \overline{f}_1^i(\sqrt{\tau}e^{y^*})f_2^i(\sqrt{\tau}e^{-y^*})] \tag{4.5}$$

and the MRS A set (no.43, 1995) of parton distribution functions[3] has been used for the PbPb and the 4 pA systems. The Monte-Carlo distributions for the SU system have been generated before the MRS A set of parton distribution functions, including the sea quark asymmetry, was available. The GRV LO set (no.4, 1992) of parton distribution functions had therefore been adopted for the SU system in ref.[4], whose results we here directly use. The adoption of two different PDF's sets in the present analysis does not influence the final results since the shapes of the generated distributions do not substantially differ and since only ratios of DY cross sections are anyway involved in the final calculations.

- *p_T differential distribution*

  The p_T differential distribution has been generated as a Bessel function of the transverse mass m_T, i.e.

$$\frac{d\sigma}{dp_T} \propto p_T m_T K_1(\frac{m_T}{T}) \tag{4.6}$$

  K_1 is the first order modified Bessel function, i.e

$$K_1(\frac{m_T}{T}) = \frac{e^{-(m_T/T)}}{\sqrt{(m_T/T)}} \cdot P_6(T/m_T) \tag{4.7}$$

  where P_6 is a polynomial of order 6 and T=0.236 GeV/c^2

- *$cos\theta_{CS}$ differential distribution*

  The experimental angular distribution has been used, i.e,

$$\frac{d\sigma}{dcos\theta_{CS}} \propto 1 + \lambda cos\theta_{CS}^2 \tag{4.8}$$

  with λ=1.

In fig.4.1 the DY generated and reconstructed mass, rapidity, cosθ_{CS} and p_T distributions are shown for the PbPb and pAl set-ups.

4.2.1 Fit of the Monte-Carlo Drell-Yan mass distribution.

The DY Monte-Carlo mass distribution has been fitted with the following functions :

- **pA**

$$\frac{dN}{dM} = par1 \cdot [e^{-a_1} + par5 \cdot e^{-a_2} + par6 \cdot e^{-a_3}] \tag{4.9}$$

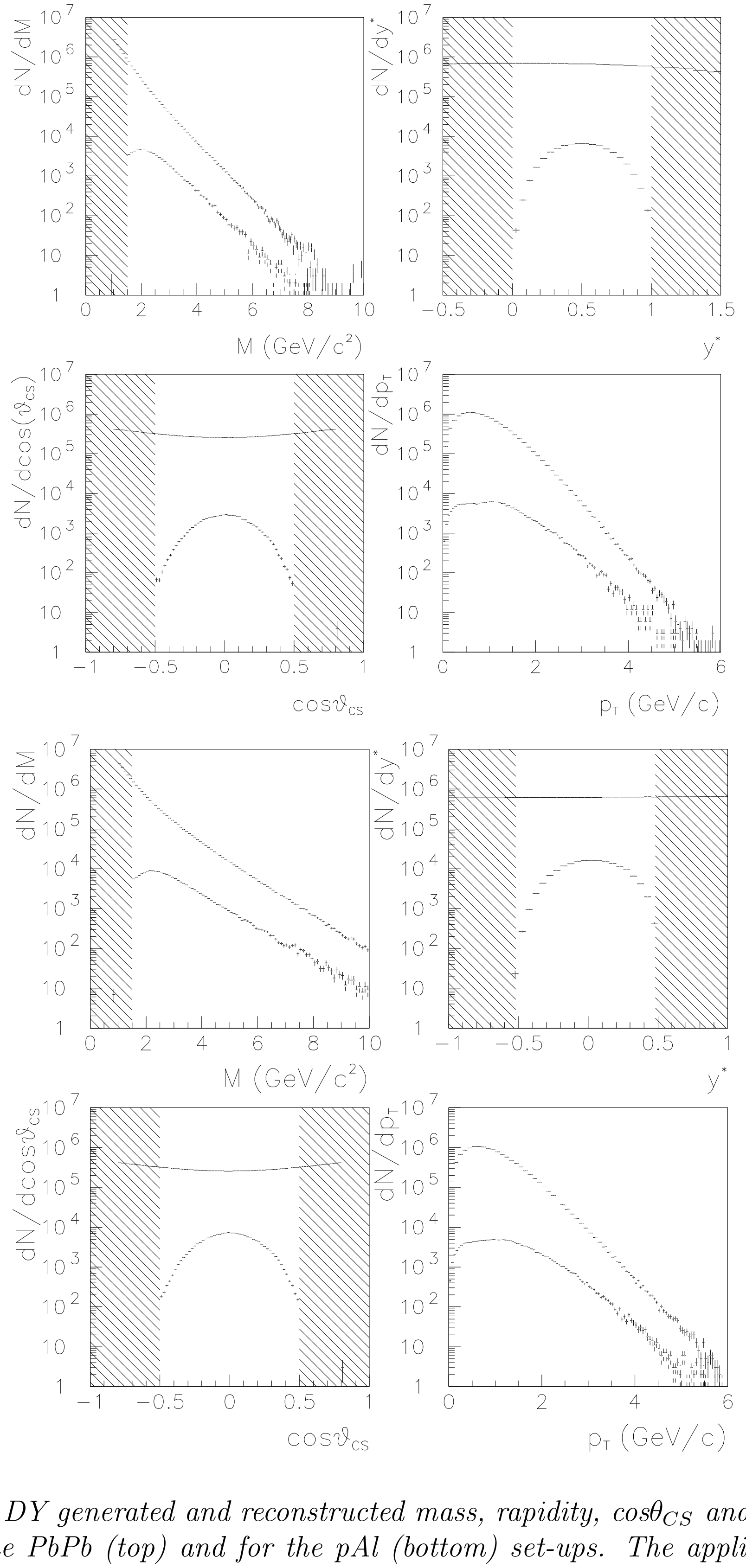

Figure 4.1: *DY generated and reconstructed mass, rapidity, $cos\theta_{CS}$ and p_T distributions for the PbPb (top) and for the pAl (bottom) set-ups. The applied kinematic cuts are represented by the shaded areas.*

system	par2 (GeV/c^2)	par3 (GeV/c^2)	par4 (GeV/c^2)	par5 $(GeV/c^2)^{-1}$	par6 $(GeV/c^2)^{-1}$
pAl	1.097±0.004	0.545±0.002	-1.299±0.002	5.15±0.08	-1.96±0.01
pCu	1.107±0.003	0.5547±0.002	-1.311±0.001	5.06±0.06	-1.97±0.01
pAg	1.116±0.003	0.5694±0.002	-1.323±0.003	5.18±0.06	-2.04±0.01
pW	1.187±0.003	0.606±0.001	-1.325±0.003	8.66±0.03	-3.26±0.01

Table 4.1: *Values of the parameters of the Monte-Carlo DY fitting function.*

System	par2 $(GeV/c^2)^{-1}$	par3 $(GeV/c^2)^{-1}$	par4 (GeV/c^2)
PbPb	1.543±0.005	0.2445±0.007	0.46±0.01

Table 4.2: *Values of the parameters of the Monte-Carlo DY fitting function.*

where

$$a_1 = M/par2 \tag{4.10}$$

$$a_2 = M/par3 \tag{4.11}$$

$$a_3 = M^2/par4^2 \tag{4.12}$$

- **AB**

$$\frac{dN}{dM} = par1 \cdot \{e^{(-par2 \cdot M)} - par3 \cdot e^{[-(M-par4)^2]}\} \tag{4.13}$$

The values of the parameters of the Monte-Carlo DY fitting functions are listed in tab.4.1 and 4.2. Since the first normalisation parameter is always left as a free parameter in the fit of the experimental mass spectrum, its value has not been listed. Fig.4.2 shows the fits of the DY mass spectrum for the pA and PbPb systems. For the SU system the results of a previous analysis[4] have been used.

4.3 The Monte-Carlo open charm generation

Since it has been verified that the PYTHIA event generator[5] well reproduces the differential distributions of D mesons produced in proton and pion induced interactions[7] (see chapter 1), the charmed meson and baryon contribution has been generated using PYTHIA 5.7. The shape of the differential charm distribution depends on the used charm mass value, on the intrinsic transverse momentum k_T

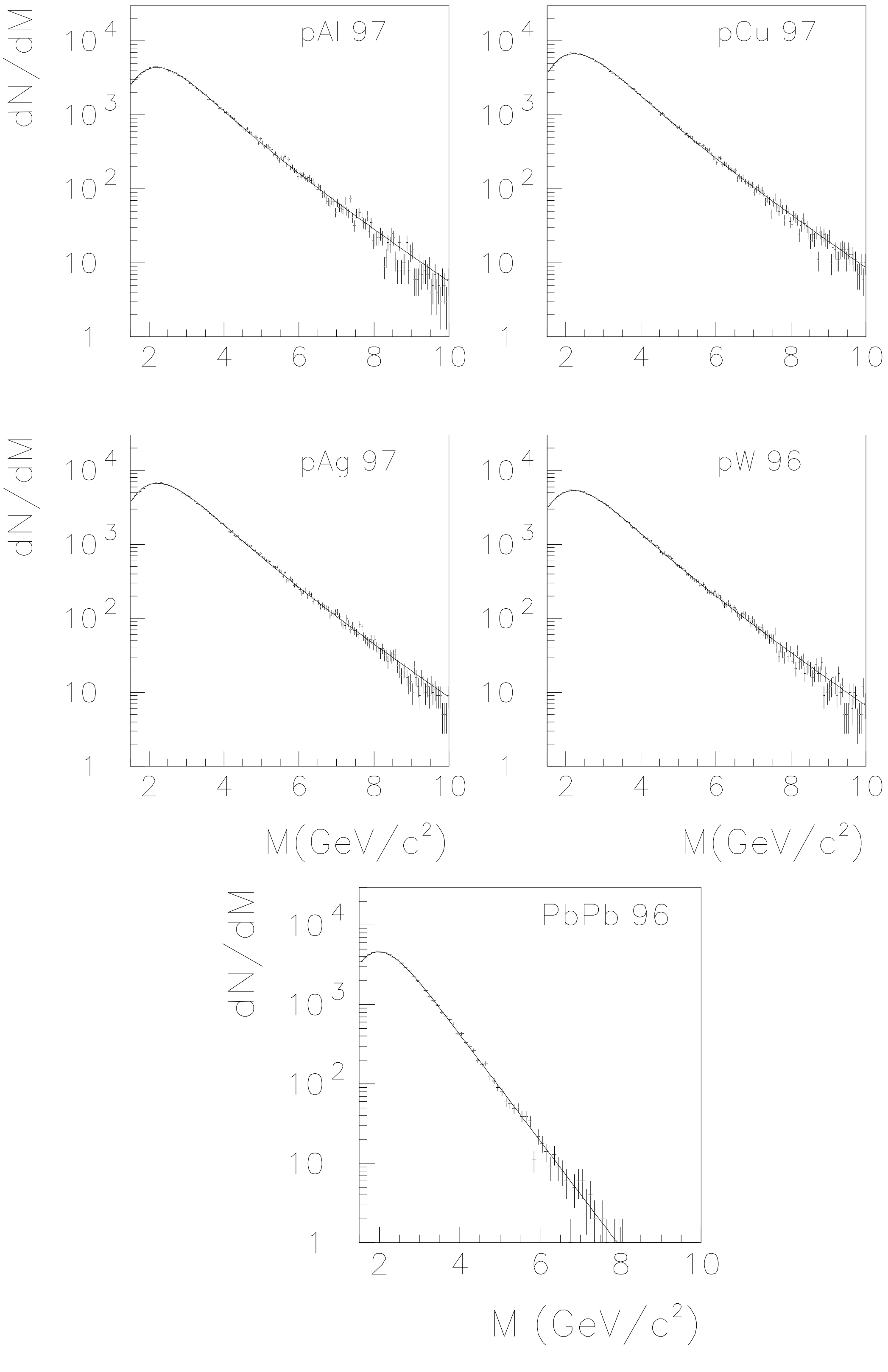

Figure 4.2: *Reconstructed and then fitted DY Monte-Carlo mass distributions for the PbPb (bottom) and the four pA set-ups (top).*

given to the incoming partons and on the chosen set of PDF's.

The commonly accepted values for the charm mass range between 1.2 up to 1.8 GeV/c^2 but the standard value m_c=1.5 GeV/c^2 seems to be favoured by experimental measurement of the $c\bar{c}$ cross section (see chapter 1). The value m_c=1.5 GeV/c^2 has been therefore used in the present work. In fig.4.3 the ratio of the Monte-Carlo mass distributions generated with $m_c = 1.2$ GeV/c^2 and $m_c = 1.5$ GeV/c^2 is shown (left) and the corresponding fitting functions are shown superimposed in the IMR region (right).

In PYTHIA, the transverse momentum of the generated charm pair originates from the intrinsic (or primordial) transverse momentum given to the colliding partons. The intrinsic transverse momentum distribution has been simulated in PYTHIA with a Gaussian k_T distribution of width σ_{k_T}, with $\langle k_T^2 \rangle = \sigma_{k_T}^2$. We have used σ_{k_T}=0.8 GeV/c, which had been previously tuned on the experimental p_T distributions by the NA38/NA50 Collaboration and was already used in order to generate the open charm component for the SU system in the analysis of ref.[4].

As far as the PDF are concerned, the same set used for the DY has been adopted.

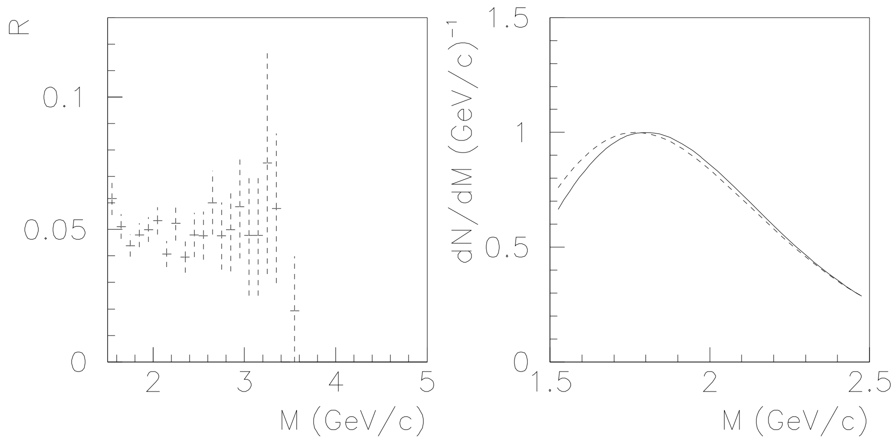

Figure 4.3: *Right : comparison of the reconstructed Monte-Carlo open charm mass spectra for Pb-Pb 158AGeV, after kinematic cuts, for* $m_c = 1.2$ *GeV/*c^2 *(dashed line) and* $m_c = 1.5$ *GeV/*c^2 *(full line). Left : ratio of the two fitting functions.*

With PYTHIA a large statistics of D^+,D^0,D_s^+ mesons and Λ_c^+, Ξ_c^0, Ξ_c^+, Ω_c^0 baryons have been generated. A 100% branching ratio has been assigned to the semi-leptonic decay channel $\longrightarrow \mu\nu_\mu X$, and 0% to all the remaining ones. The Monte-Carlo distributions of open charm dimuons are then weighted with the real branching ratios listed in tab.4.3. This procedure avoids the use of enormous CPU time, since we impose that all the generated mesons and baryons effectively decay into a muon.

open charm state	$B.R.(H_{(c)} \rightarrow \mu\overline{\nu}_{mu}X)$
$D^{\pm}$	0.172 ± 0.019
D^0	0.066 ± 0.008
D^s	$0.08 + 0.06 - 0.05$
Baryons	0.045 ± 0.017

Table 4.3: *Total B.R. of charmed hadrons H_c in the semi-leptonic decay channel ($\rightarrow \mu\overline{\nu}_{mu}X$)[6].*

In fig.4.4 the reconstructed differential mass distribution of open charm dimuons for the PbPb system is shown with and without branching ratio weighting.

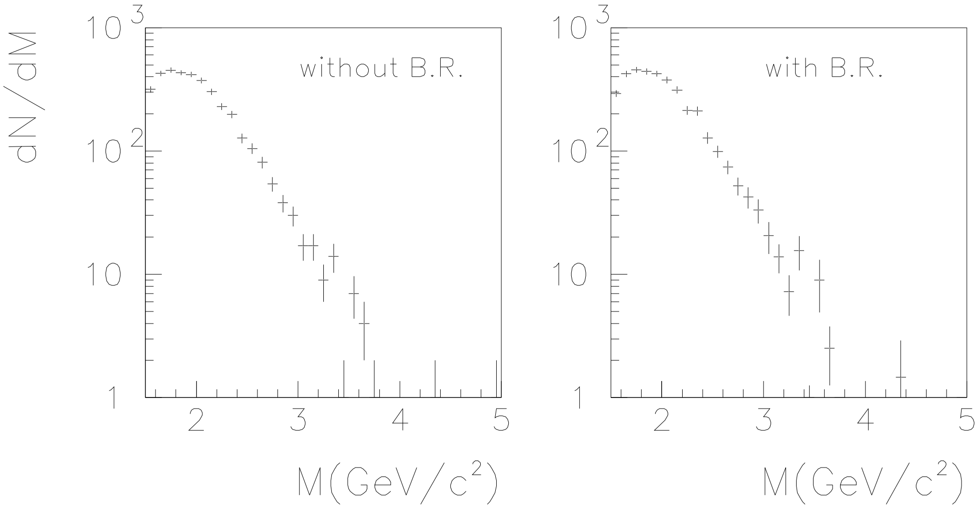

Figure 4.4: *Reconstructed mass distributions of open charm dimuons for the PbPb system before (left) and after (right) branching ratio weighting. The area of the weighted distribution has been renormalised to the unweighted one.*

In fig.4.5 the generated and reconstructed mass, rapidity, p_T and $\cos\theta_{CS}$ differential distributions of open charm dimuons are shown for the pA and PbPb set-ups. Branching ratio weighting has been applied and kinematic cuts imposed on the reconstructed distributions.

4.3.1 Fit to the Monte-Carlo open charm mass distribution

The Monte-Carlo mass differential distribution of open charm dimuons has been fitted with the following function :

$$\frac{dN}{dM} = par1 \cdot e^{\{-0.5 \cdot [(M - par2)/\sigma]^2\}} \tag{4.14}$$

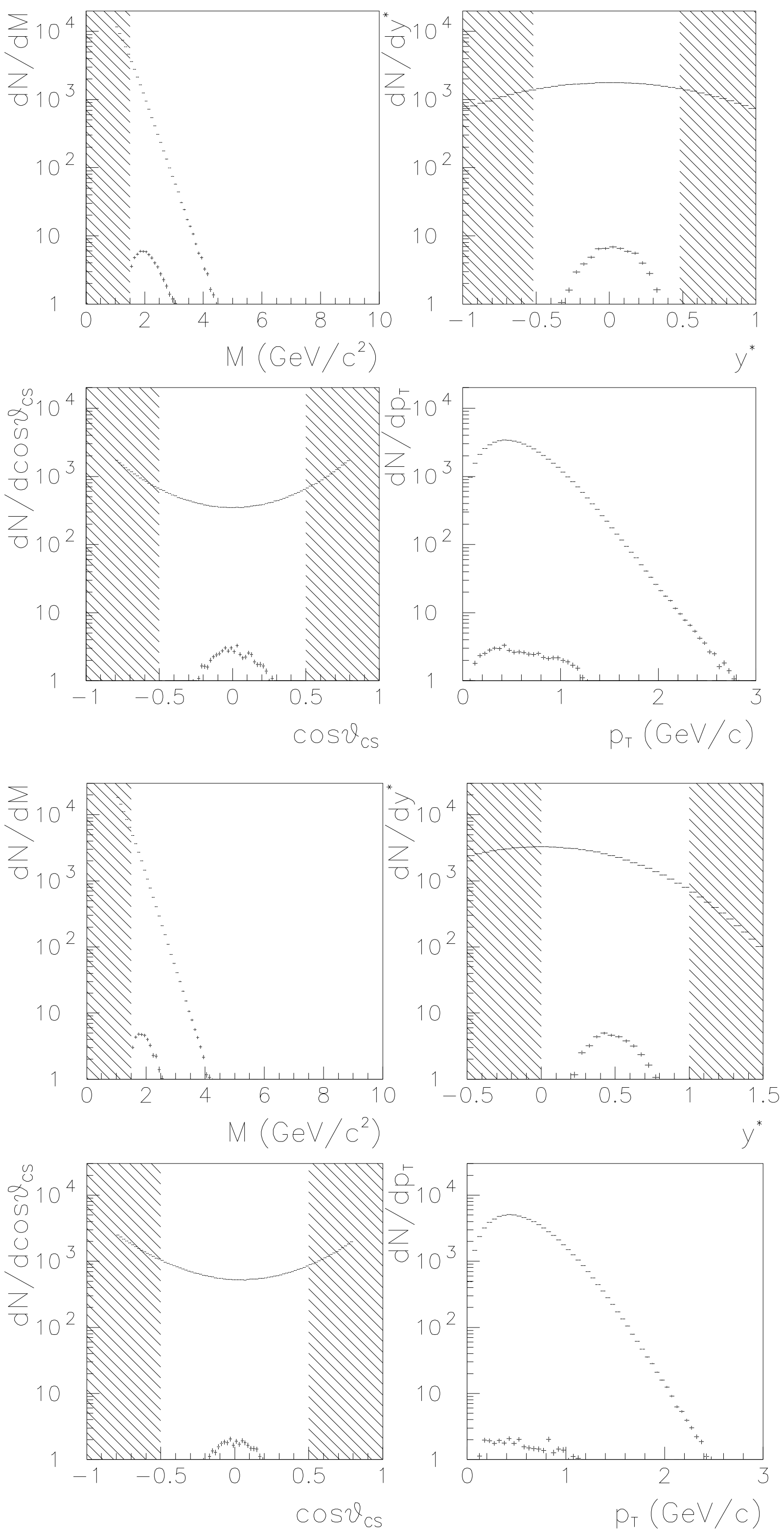

Figure 4.5: *Generated ($m_c = 1.5$ GeV/c^2) and reconstructed mass, rapidity, $cos\theta_{CS}$ and p_T distributions of open charm dimuons for the pAl (top) and PbPb (bottom) set-ups. B.R. weighting has been applied. The applied kinematic cuts are represented by the shaded areas.*

System	par2 (GeV/c^2)	par3 (GeV/c^2)	par4 $(GeV/c^2)^{-1}$	par5 (GeV/c^2)
pAl	1.931±0.009	0.37±0.02	0.35±0.04	1.5±0.1
pCu	1.975±0.007	0.35±0.03	0.34±0.03	1.3±0.2
pAg	1.997±0.008	0.37±0.03	0.38±0.03	1.8±0.2
pW	1.933±0.008	0.37±0.032	0.35±0.03	1.5±0.3
PbPb	1.800±0.01	0.30±0.04	0.42±0.06	1.5±0.3

Table 4.4: *Values of the parameters of the Monte-Carlo open charm fitting function.*

where

$$\sigma = \begin{cases} par3 & \text{for } M < par5 \\ par3[1 + par4(M - par5)] & \text{for } M > par5 \end{cases} \tag{4.15}$$

Fig.4.6 shows the fit of the pA and PbPb reconstructed open charm mass distributions. Branching ratio weighting has been applied and the shown distributions have been renormalised to the unweighted ones.
Table 4.4 lists the values of the parameters of the Monte-Carlo open charm fitting functions. The values of the SU parameters have been taken from reference[4].

4.4 The Monte-Carlo J/ψ and ψ' simulation

The J/ψ and ψ' Monte-Carlo mass distributions have been obtained using the following parametrisations :

- *Mass differential distribution*

$$M_{J/\psi} = 3.097\ GeV/c^2 \tag{4.16}$$

$$M_{\psi'} = 3.686\ GeV/c^2 \tag{4.17}$$

- *Rapidity differential distribution*

  Gaussian with

$$\mu_{y^*} = 0 \tag{4.18}$$

  and

$$\sigma_{y^*} = 0.6 \tag{4.19}$$

- *Transverse momentum distribution*

  The same p_T distribution used for the DY.

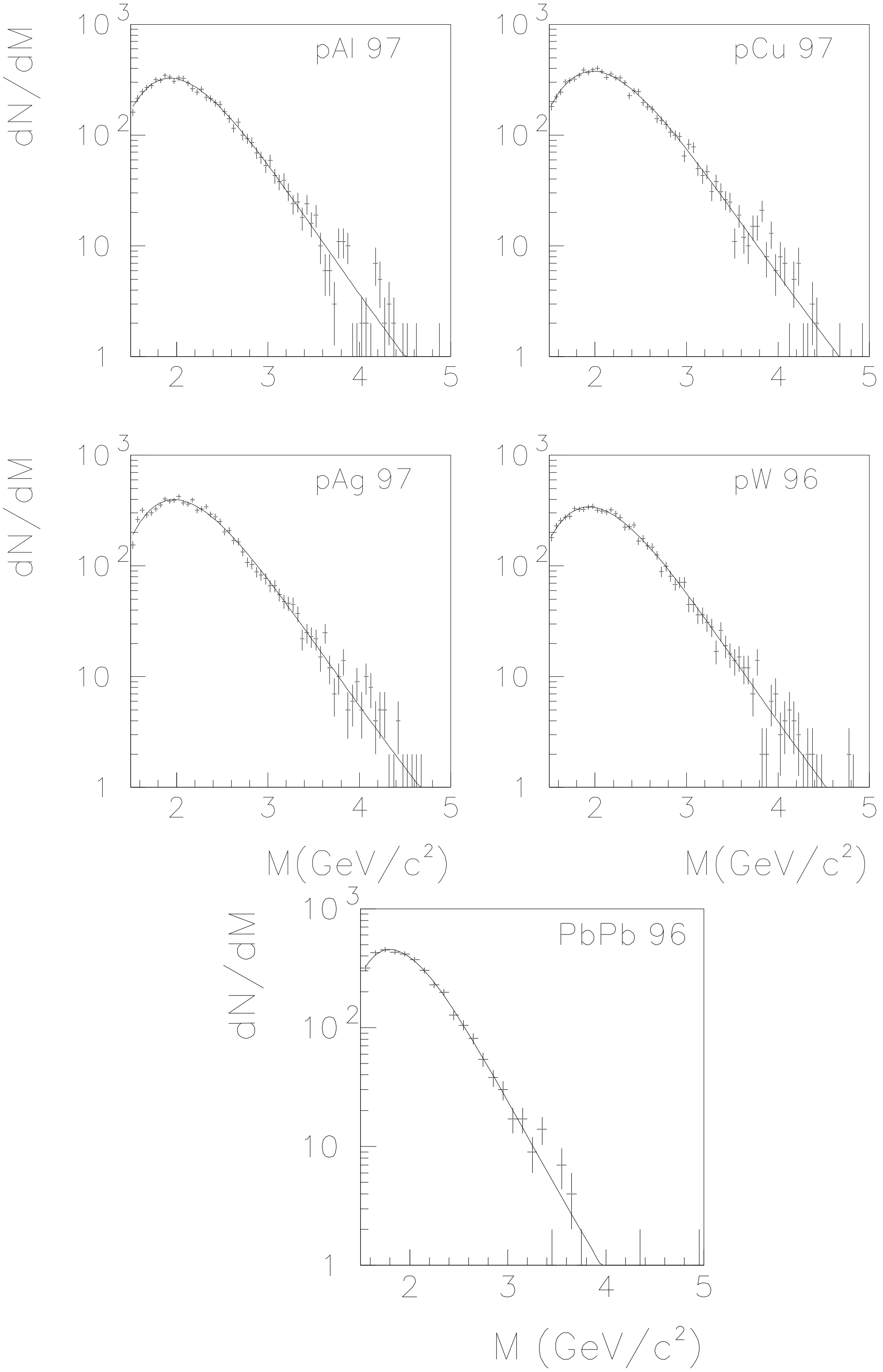

Figure 4.6: *Fit of the Monte-Carlo generated and then reconstructed pA (top) and PbPb (bottom) mass distributions of dimuons from open charm decays.*

- $\cos\theta_{CS}$ *distribution*

  Uniform distribution in $\cos\theta_{CS}$

In 4.7 the J/ψ generated and reconstructed mass, rapidity, p_T and cosθ_{CS} distributions are shown for the pAl and PbPb set-ups. The same is shown in fig.4.8 for the ψ'.

4.4.1 Fit of the Monte-Carlo J/ψ and ψ' mass distributions

The reconstructed mass differential distributions have been fitted with the following functions :

$$\frac{dN}{dM} = par1 \cdot e^{\{-0.5\cdot[((M-par2)/\sigma)^2]\}} \tag{4.20}$$

where

$$\sigma = \begin{cases} par3 & \text{for M}\geq M_1 \text{ and M}\leq M_2 \\ par3\{1+[par4(M_1-M)]\}^{[par5-par6(M_1-M)^\alpha]} & \text{for M}\leq M_1 \\ par3\{1+[par7(M-M_2)]\}^{[par8-par9(M-M_2)^\beta]} & \text{for M}\geq M_2. \end{cases} \tag{4.21}$$

and

$$M_1 = par10 \cdot par2 \tag{4.22}$$

$$M_2 = par11 \cdot par2 \tag{4.23}$$

The same functions have been used for the J/ψ and the ψ'. The α and β coefficients listed in tab.4.8 have been determined case by case in order to obtain the best possible fit. Table 4.5, 4.6 and 4.7 list the values of the parameters of the Monte-Carlo J/ψ and ψ' fitting functions.
In fig.4.9 and 4.10 the recontructed and then fitted J/ψ and ψ' mass differential distributions are shown for the pA and PbPb set-ups.

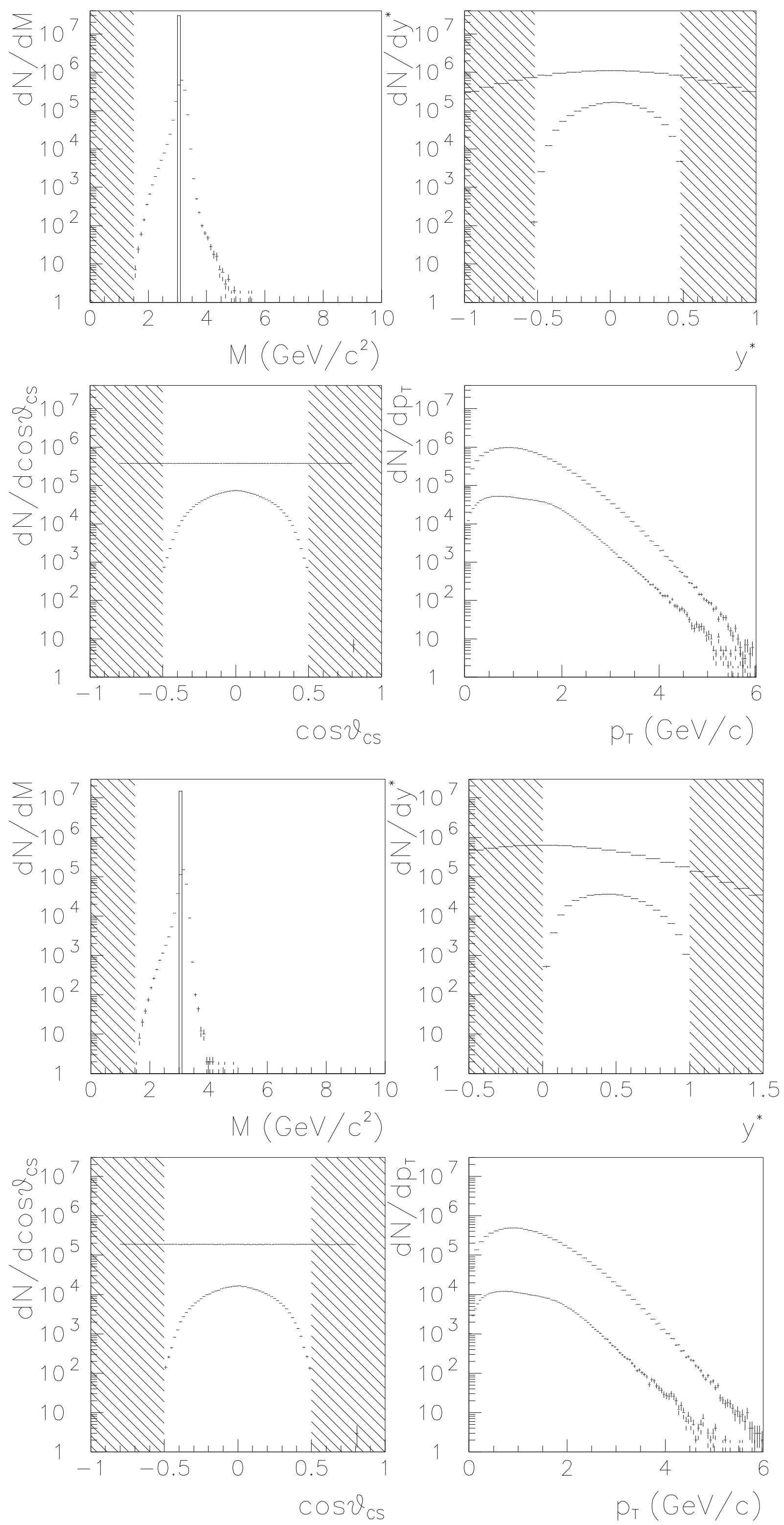

Figure 4.7: *Generated and reconstructed J/ψ mass, rapidity, $cos\theta_{CS}$ and p_T distributions for the pAl (top) and PbPb (bottom) set-ups. The applied kinematic cuts are represented by the shaded areas.*

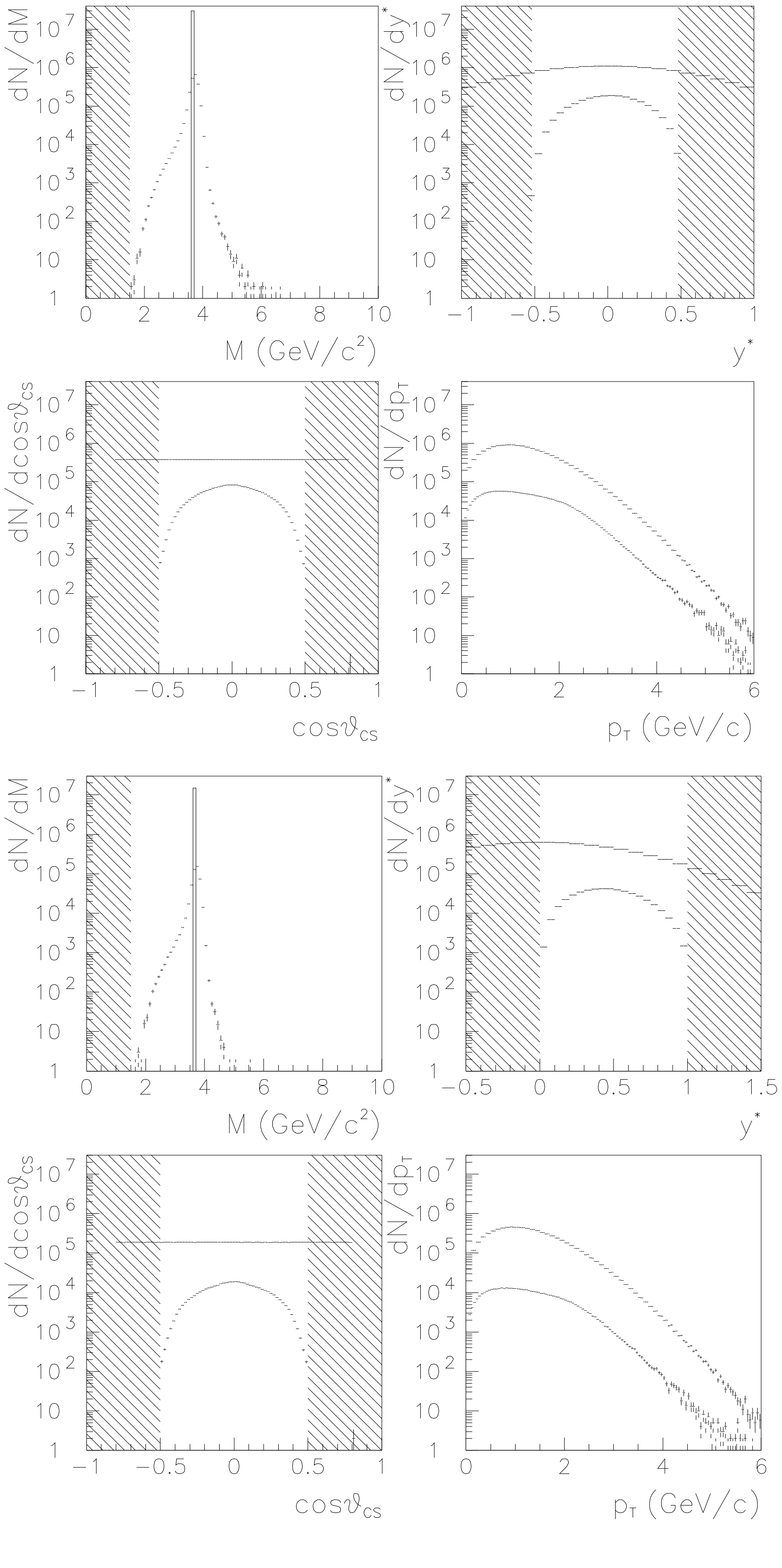

Figure 4.8: *Generated and reconstructed ψ' mass, rapidity, $cos\theta_{CS}$ and p_T distributions for the pAl (top) and PbPb (bottom) set-up. The applied kinematic cuts are represented by the shaded areas.*

	pAl	pCu	pAg	pW
par2(GeV/c^2)	3.133±0.1E-3	3.139±0.3E-3	3.142±0.3E-3	3.146±0.3E-3
par3(GeV/c^2)	0.1027±0.1E-3	0.1070±0.3E-3	0.112±0.3E-3	0.107±0.2E-3
par4$(GeV/c^2)^{-1}$	1.934±0.004	0.273±0.006	0.273±0.004	1.829±0.009
par5	1.404±0.005	1.322±0.002	1.355±0.002	1.39±0.02
par6$(GeV/c^2)^{-\alpha}$	0.455±0.007	1.741±0.004	1.724±0.003	0.43±0.01
par7$(GeV/c^2)^{-1}$	1.479±0.009	1.31±0.01	1.24±0.03	1.383±0.004
par8	1.50±0.02	2.07±0.06	2.1±0.1	1.50±0.02
par9$(GeV/c^2)^{-\beta}$	0.30±0.02	0.77±0.08	0.8±0.1	0.21±0.02
par10	0.9659±0.1E-3	0.976±0.001	0.976±0.001	0.965±0.001
par11	1.070±0.001	1.049±0.001	1.046±0.006	1.059±0.001

Table 4.5: *Values of the parameters of the Monte-Carlo J/ψ fitting functions for the pA set-ups.*

	pAl	pCu	pAg	pW
par2(GeV/c^2)	3.727±0.1E-3	3.730±0.3E-3	3.735±0.3E-3	3.740±0.1E-3
par3(GeV/c^2)	0.1119±0.1E-3	0.1158±0.3E-3	0.1216±0.4E-3	0.1158±0.1E03
par4$(GeV/c^2)^{-1}$	0.1689±0.9E-3	0.160±0.002	0.162±0.002	0.170±0.001
par5	1.0370±0.5E-3	0.996±0.003	1.009±0.004	1.049±0.6E-3
par6$(GeV/c^2)^{-\alpha}$	1.402±0.001	1.328±0.004	1.316±0.006	1.391±0.001
par7$(GeV/c^2)^{-1}$	1.305±0.008	1.16±0.01	1.07±0.01	1.248±0.006
par8	1.57±0.03	2.78±0.09	2.79±0.07	1.51±0.02
par9$(GeV/c^2)^{-\beta}$	0.27±0.02	1.5±0.1	1.5±0.2	0.173±0.009
par10	0.9699±0.4E-3	0.9667±0.8E-3	0.963±0.001	0.968±0.4E03
par11	1.060±0.002	1.034±0.002	1.028±0.002	1.054±0.001

Table 4.6: *Values of the parameters of the Monte-Carlo ψ' fitting functions for the pA set-ups.*

	PbPb	PbPb
	J/ψ	ψ'
par2(GeV/c^2)	3.126±0.2E-3	3.718±0.2E-3
par3(GeV/c^2)	0.090±0.1E-3	0.102±0.2E-3
par4$(GeV/c^2)^{-1}$	0.227±0.001	0.168±0.1E-2
par5	1.131±0.001	1.006±0.9E-3
par6$(GeV/c^2)^{-\alpha}$	1.655±0.002	1.436±0.002
par7$(GeV/c^2)^{-1}$	0.18±0.01	0.21±0.01
par8	1.041±0.005	1.256±0.006
par9$(GeV/c^2)^{-\beta}$	1.35±0.01	1.51±0.01
par10	0.9817±0.2E-3	0.9729±0.6E-3
par11	1.073±0.001	1.066±0.002

Table 4.7: *Values of the parameters of the Monte-Carlo J/ψ and ψ' fitting functions for the PbPb set-up.*

System	$\alpha_{J/\psi}$	$\beta_{J/\psi}$	$\alpha_{\psi'}$	$\beta_{\psi'}$
pAl	1.0	1.0	0.5	1.0
pCu	0.5	0.5	0.5	0.5
pAg	0.5	0.5	0.5	0.5
pW	1.0	1.0	0.5	1.0
PbPb	0.5	0.5	0.5	0.5

Table 4.8: *Values of the coefficients α and β of the Monte-Carlo J/ψ and ψ' fitting functions.*

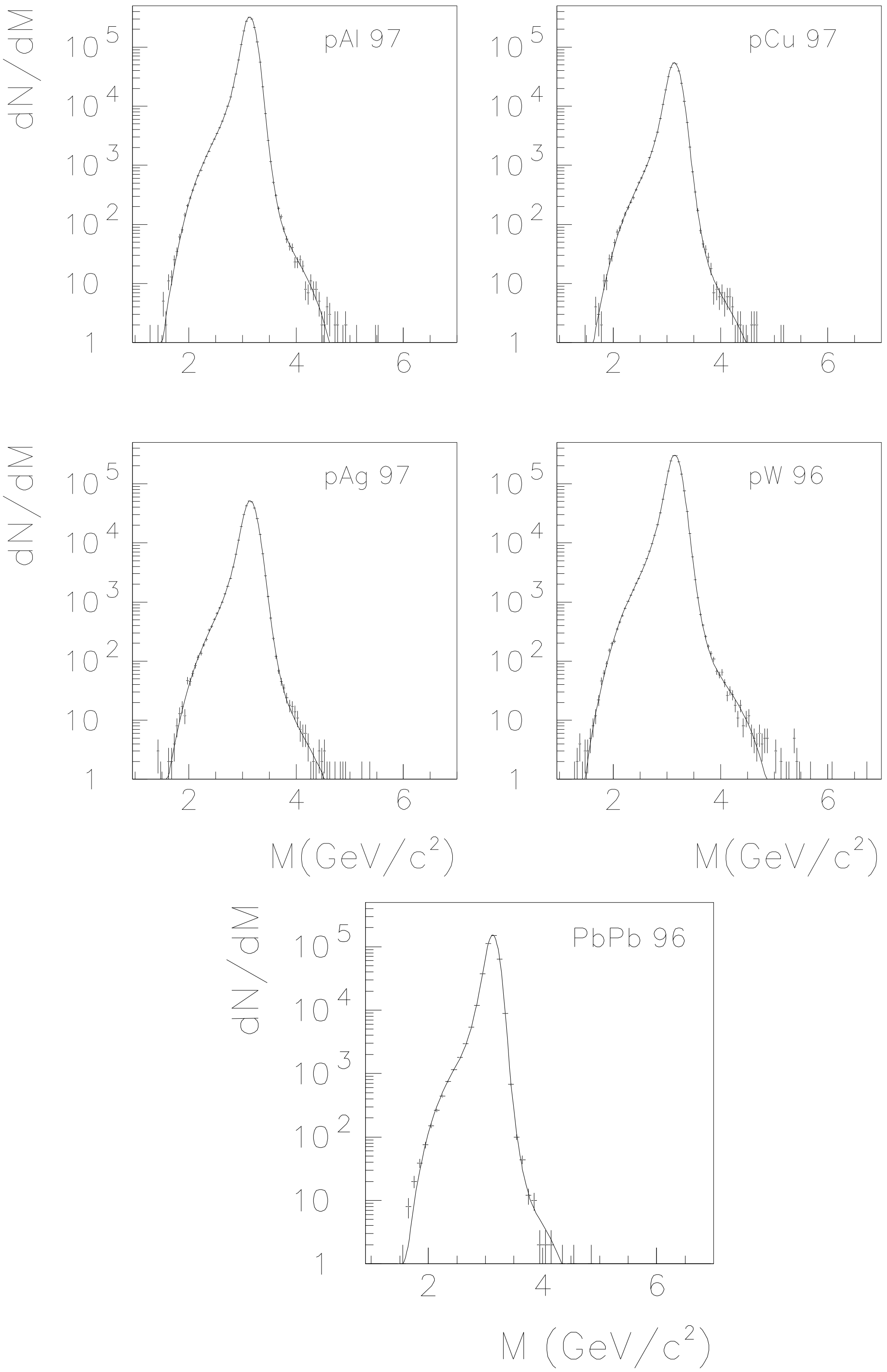

Figure 4.9: *Fit of the reconstructed J/ψ Monte-Carlo mass distributions for the 4 pA (top) and the PbPb (bottom) set-ups.*

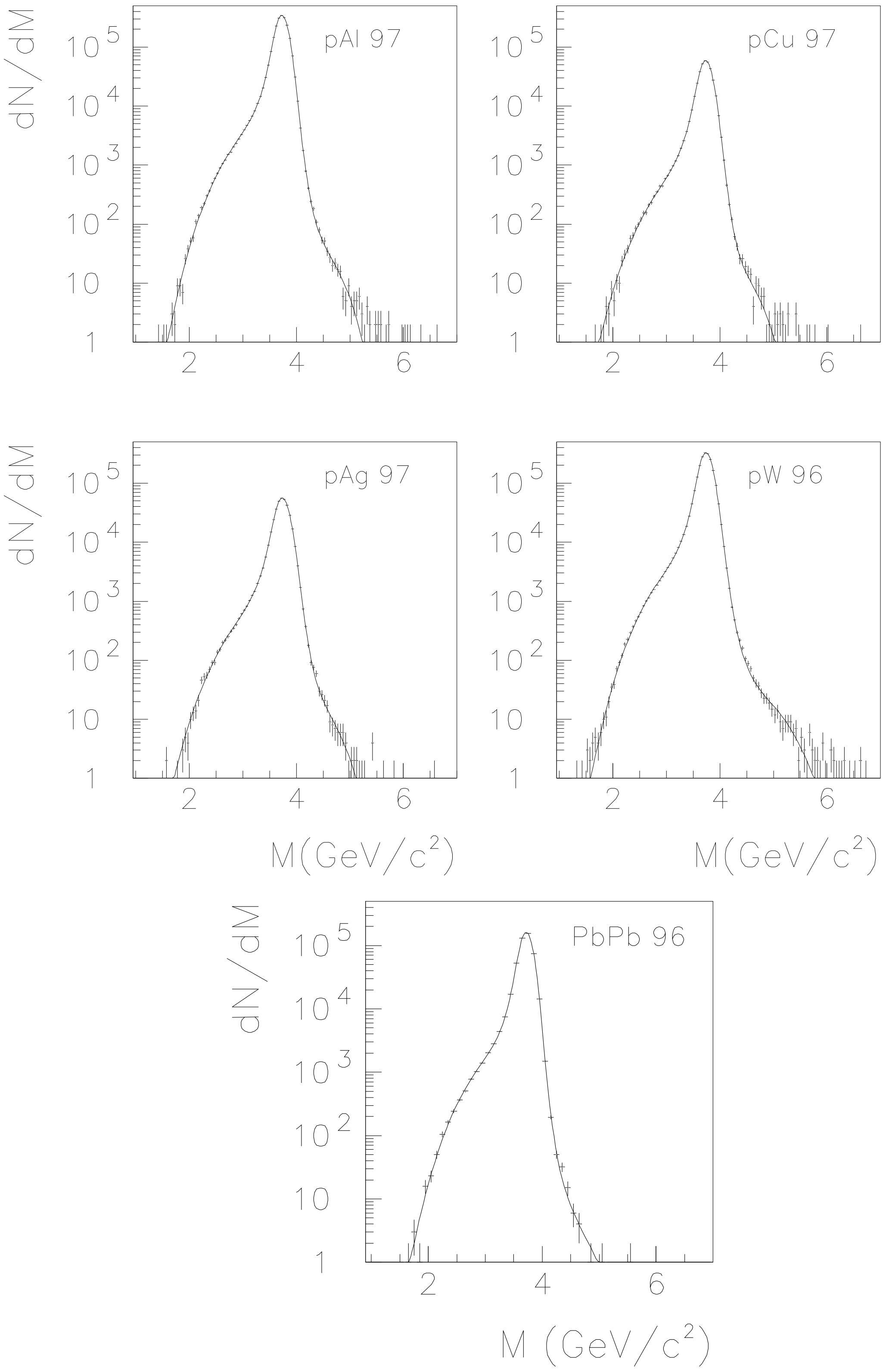

Figure 4.10: *Fit of the reconstructed ψ' mass distributions for the 4 pA (top) and the PbPb (bottom) set-ups.*

System	A_{DY} %	$A_{D\overline{D}}$ %	$A_{J/\psi}$ %	$A_{\psi'}$ %
	$M > 1.5\ GeV/c^2$	$M > 1.5\ GeV/c^2$		
pAl	6.08±0.01	2.04±0.02	14.50±0.01	16.96±0.01
pCu	6.56±0.01	1.84±0.02	14.99±0.03	17.55±0.03
pAg	6.42±0.01	1.92±0.02	14.94±0.03	17.49±0.03
pW	6.19±0.01	2.14±0.02	14.44±0.01	16.80±0.01
PbPb	2.81±0.01	1.08±0.02	7.44±0.01	8.69±0.01

Table 4.9: *Calculated acceptances (in %) for the indicated physical process.*

4.5 Acceptances

The acceptance of the apparatus for a given physical process is defined as the ratio of the numbers of Monte-Carlo reconstructed and generated events,e.g. :

$$A = \frac{\int_{M_1}^{M_2} \frac{dN^{rec}}{dM}\, dM}{\int_{M_1}^{M_2} \frac{dN^{gen}}{dM}\, dM} \tag{4.24}$$

when the rapidity and $\cos\theta_{CS}$ kinematic cuts have been applied on both distributions. For DY and open charm M_1=1.5 GeV/c^2 and M_2 is the upper value of the mass range covered by the considered process, whereas the whole mass distributions of the J/ψ and ψ' have been integrated. Tab.4.9 lists the acceptances for the physical processes discussed in the present chapter.

Bibliography

[1] DIMUJET USER GUIDE 2.00/02 (1997)

[2] DIMUREC USER GUIDE 2.00/02 (1997)

[3] PDFLIB 7.09, Users's Manual, CERN/PPE (1997)

[4] A.Borhani, Ph.D. Thesis, Uni. Paris 6 (1996)

[5] T.Sjostrand, Pythia 5.7 and Jetset 7.4 (1993)

[6] C.Caso et al., Review of Particle Physics, The European Physical Journal C3 (1998)1.

[7] P.Braun-Munzinger et al., CERN-PPE/97-65 (1997) subm. Z.Phys.C